Радиофизика и радиоастрономия, 2008, т. 13, №2, с. 120-137

Earth – Atmosphere – Geospace as an Open Nonlinear Dynamical System

L. F. Chernogor and V. T. Rozumenko

Kharkiv V. Karazin National University,
4, Svoboda Sq., Kharkiv, 61077, Ukraine
E-mail: Leonid.F.Chernogor@univer.kharkov.ua

Received November 13, 2007

The concept of the Earth-atmosphere-ionosphere-magnetosphere (EAIM) system as a complex open dissipative nonlinear dynamical system whose most important property is trigger mechanisms for energy releases has been validated, the basic aspects of the system paradigm being stated. Highly energetic phenomena in the system have been shown to give rise to a complex cluster of processes and to the reconstruction in the subsystem coupling. The active experiments in the EAIM system have established the limitation of the linear description of the subsystem response to large energy inputs, determined the possibility of the onset of large-scale and global-scale perturbation from local and localized energy releases, as well as revealed and identified the types of waves transferring these disturbances. The majority of highly variable processes in the EAIM system have been determined to be accompanied by energetic particle precipitations from the magnetosphere at middle latitudes.

1. Introduction

A major achievement of the physics of the Earth, atmosphere, and geospace over the last quarter of the twentieth century has been the realization that a proper understanding of the processes acting in all spheres of our planet, and hence physics-based modeling, is impossible within the old paradigm where all spheres are considered separately, and even when coupling between two spheres is accounted for, it is considered to be linear. The instantaneous state of any sphere has turned out to be insufficient to predict its future evolution.

Chernogor [1-4] have formulated and developed the basics for the system paradigm in the 1980th. These papers present the validation of the concept that the Earth-atmosphere-ionosphere-magnetosphere (EAIM) system is an open, dynamic, and, above all, nonlinear system with inherent non-trivial properties. Data on this system, distinct from data on a subsystem, permit more reliable forecasting of its state.

The goal of this work is a formulation of the basic aspects of the system paradigm for the EAIM system and the discussion of the principle processes operating there.

2. The Basic Aspects of the System Paradigm

(1) The Earth and the near-Earth environment constitute a unified system. It consists of subsystems, internal and external spheres. This study is concerned with the tectonosphere, atmosphere, ionosphere, and magnetosphere forming the TAIM system, and the ocean, atmosphere, ionosphere, and magnetosphere, forming the OAIM system, both of which form the EAIM system. The EAIM system has a hierarchical structure.

(2) The EAIM system constituents interact via a myriad of various (direct, feedback, positive, negative, and in combination with each other) mechanisms, as illustrated in Figure 1.

(3) The EAIM system is open. Emissions, matter, energy are supplied from above and below, which give rise to entropy production, as the data in Tables 1 and 2 show.

(4) The EAIM system is dynamic. Its parameters vary in space and time. Consequently, the system is governed by partial differential equations satisfying the initial and boundary conditions, which are known with finite errors.

(5) The EAIM system is nonlinear, which is a consequence of the high-energy processes acting in it, as the data presented in Tables 3 and 4 illustrate, and the nonlinearities, in turn, drive instabilities, produce irregularities, generate intense waves, etc.

(6) The Earth and its envelopes have the property of self-developing, complicating, and developing self-organizing patterns owing to the influx of energy, emissions, mass, etc.

3. Processes Acting in the EAIM system

3.1. Geospace Storms

Coronal mass ejections cause the most fundamental rearrangement of processes operating in the EAIM system, geospace storms, as depicted in Figure 1. The geospace storm is termed to be a set of storms including the magnetic, ionospheric, atmospheric, and electric ones [1-3, 5-9].

The geospace storm could apparently be responsible for the onset of high-energy processes occurring in the troposphere, such as the hurricane, with a triggering factor of $\sim 10^9 \div 10^{10}$ [1-4].

The geospace storm characteristics are presented in Table 5.

The magnetic storm energy, ΔE_m, can be estimated in terms of disturbances in the geomagnetic flux density, ΔB, and can vary in a wide range of values, as illustrated in Table 6. The magnetic storm power, P_m, also depends on

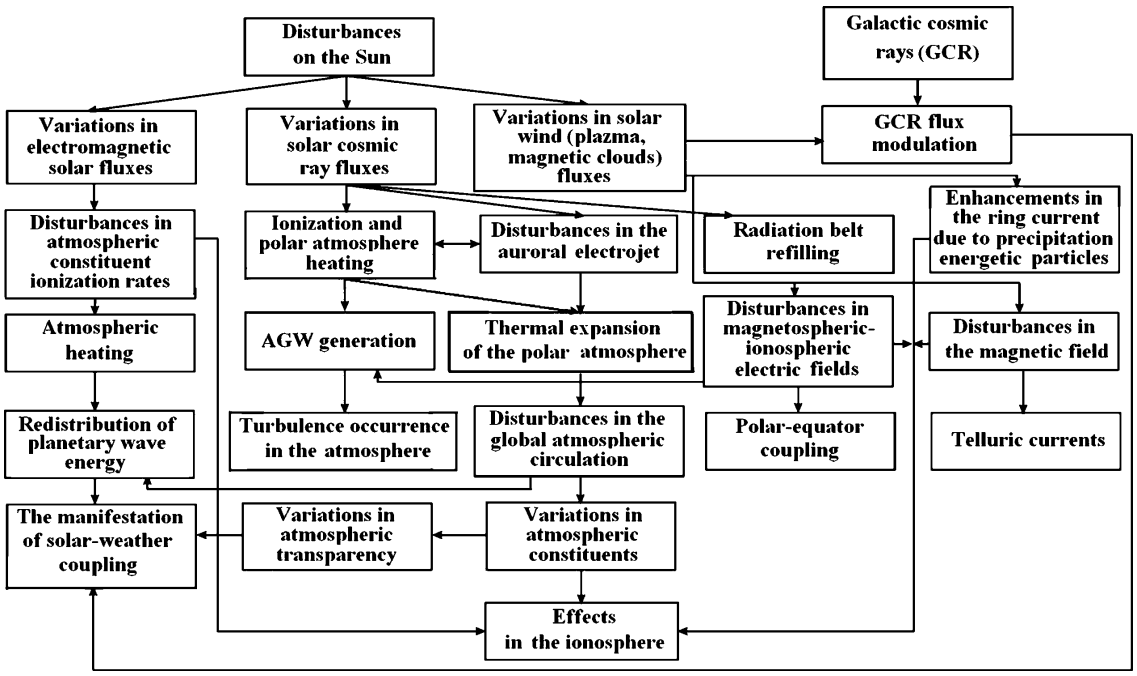

Fig. 1. *Processes accompanying geospace storms and variations in space weather (AGW are acoustic-gravity waves)*

Table 1. *The energetics of fluxes from above*

Source	Π_P (W/m^2)	Area (m^2)	P (W)	Duration (s)	Comments
Solar emissions under quiet conditions:					Wavelength:
optical	1400	$1.3\cdot10^{14}$	$1.8\cdot10^{17}$	Continuously	$\lambda\approx0.4\div0.8$ μm
ultraviolet – soft X-rays	$\sim2\cdot10^2$	$1.3\cdot10^{14}$	$\sim3\cdot10^{16}$		$\lambda\approx1\div180$ nm
hard X-rays	$\sim10^{-8}$	$1.3\cdot10^{14}$	$\sim10^6$		$\lambda\approx0.1\div1$ nm
Solar emissions under disturbed conditions:					
optical	1400	$1.3\cdot10^{14}$	$1.8\cdot10^{17}$	$\sim10^2$	$\lambda\approx0.4\div0.8$ μm
ultraviolet – soft X-rays	$\sim2\cdot10^2$	$1.3\cdot10^{14}$	$\sim3\cdot10^{16}$	$\sim10^2$	$\lambda\approx1\div180$ nm
hard X-ray	$\sim5\cdot10^{-4}$	$1.3\cdot10^{14}$	$\sim6.5\cdot10^{10}$	$\sim10^2$	$\lambda\approx0.1\div1$ nm
Solar protons:					Proton energy: $10\div100$ MeV
under quiet conditions	0.1	10^{16}	10^{15}	Continuously	Flux: $10^{11}\div10^9$ m$^{-2}\cdot$s^{-1}
under disturbed conditions	$2\div3$	10^{16}	$(2\div3)\cdot10^{16}$	$10^2\div10^5$	Flux: $(2\div3)\cdot10^{12}$ m$^{-2}\cdot$s^{-1}
Solar wind:					
quiet	$6\cdot10^{-5}$	10^{16}	$6\cdot10^{11}$		$N_p\approx5\cdot10^6$ m^{-3}, $\upsilon_p\approx400$ km/s
disturbed	$5\cdot10^{-2}$	10^{16}	$5\cdot10^{14}$	$(4\div30)\cdot10^4$	$N_p\approx10^8$ m^{-3}, $\upsilon_p\approx1000$ km/s
Galactic cosmic rays	10^{-6}	$\sim10^{14}$	10^8	Continuously	Flux: 10^4 m$^{-2}\cdot$s^{-1} Proton energy: $\varepsilon_p=1$ GeV
Meteoroid flux:					Particle mass:
background	$5\cdot10^{-7}$	$\sim10^{14}$	$5\cdot10^7$	Continuously	$m\geq10^{-10}$ kg
maximum flux	$5\cdot10^{-2}$	$\sim10^{14}$	$\sim5\cdot10^{12}$	$10^3\div10^4$	Same as above
Precipitating energetic particles:					
under quiet conditions	10^{-4}	$\sim10^{13}$	10^9	$10^2\div10^4$	High latitudes
under disturbed conditions	1	$\sim10^{13}$	$\sim10^{13}$	$10^2\div10^4$	Same as above
Infrared thermospheric emissions:					$\lambda=2\div10$ μm Stronger at high latitudes
under quiet conditions	$10^{-3}\div10^{-2}$	$5\cdot10^{14}$	$(5\div50)\cdot10^{11}$	Continuously	
under disturbed conditions	$0.1\div1$	$5\cdot10^{14}$	$(5\div50)\cdot10^{14}$	$10^2\div10^4$	

Here, Π_P is the energy flux density, P is the power of processes

both a ΔE_m value and the duration Δt of the storm's main phase.

We advance a new classification of geospace storms in terms of their constituent intensity, as presented in Table 7.

3.2. Seismic Processes

An earthquake was the first high-energy source that caused a significant revision of earlier ideas about the role of energy fluxes from below. The energy and power of the most vio-

Table 2. *The energetics of fluxes from below*

Source	Π_P (W/m^2)	Area (m^2)	P (W)	Duration (s)	Comments
Earth's surface infrared emissions	$4\cdot10^2$	$5\cdot10^{14}$	$2\cdot10^{17}$	Continuously	Absorbed and radiated by the atmosphere
Water vapor	80	$5\cdot10^{14}$	$4\cdot10^{16}$	Same as above	Latent heat released from atmospheric water vapor
Air convection	30	$5\cdot10^{14}$	$1.5\cdot10^{16}$	Same as above	—
Heat fluxes from the Earth's interior	$6\cdot10^{-2}$	$5\cdot10^{14}$	$3\cdot10^{13}$	Same as above	Plays negligible role
Atmospheric turbulence	$1\div10$	$5\cdot10^{14}$	$(5\div50)\cdot10^{14}$	Same as above	Up to $\sim100\div120$ km altitude
Internal gravitational waves (IGW)	$0.1\div1$	$5\cdot10^{14}$	$(5\div50)\cdot10^{13}$	Same as above	Effectively dissipated in the thermosphere
Tidal waves	10^{-3}	$5\cdot10^{14}$	$5\cdot10^{11}$	Same as above	Same as above
Planetary waves	10^{-3}	$5\cdot10^{14}$	$5\cdot10^{11}$	Same as above	Same as above
Infrasound	$10^{-4}\div10^{-3}$	$5\cdot10^{14}$	$(5\div50)\cdot10^{10}$	Same as above	Reach the ionospheric F region
Infrasound from the strongest earthquake	$10^2\div10^3$	10^{11}	$10^{13}\div10^{14}$	10^2	Same as above
Electromagnetic emissions from the strongest earthquake	$10^{-3}\div10^{-2}$	10^{11}	$10^8\div10^9$	$10^2\div10^3$	Reach the ionosphere and magnetosphere
Acoustic emissions from the most powerful lightning discharge	10^{-3}	10^9	10^6	~1	Dissipated in the atmosphere
Electromagnetic emissions from the most powerful lightning discharge	10^{-3}	10^9	10^6	~1	Reach the ionosphere and magnetosphere
Acoustic emissions from global thunderstorm activity	10^{-3}	10^{12}	10^9	Continuously	Dissipated in the atmosphere
Electromagnetic emissions from global thunderstorm activity	10^{-3}	10^{12}	10^9	Same as above	Reach the ionosphere and magnetosphere

lent earthquakes can attain values of $\sim10^{19}$ J and $\sim10^{17}$ W, respectfully.

Earthquakes exert their influence on the geospace environment via the following four channels: (1) acoustic-gravity waves, (2) quasi-steady electric and magnetic fields, (3) electromagnetic waves generated by variations in strain at boundaries between the mobile lithospheric plates, (4) MHD waves generated at altitudes of the dynamo region via the modulation of the current flows by the acoustic-gravity waves from earthquakes and via the modulation of the ionospheric electric field by the electric field from earthquakes.

Table 3. *Parameters of natural processes in the EAIM system*

Source	Energy (J)	Power (W)	Impact duration (s)	Comments
Solar optical emissions	10^{22}	10^{17}	10^5	During 24 hours
Solar wind	10^{17}	10^{12}	10^5	Same as above
Meteorite	$10^{12} \div 10^{15}$	$10^{11} \div 10^{15}$	$1 \div 10$	Affects the atmosphere
Asteroid	$10^{15} \div 10^{26}$	$3 \cdot 10^{18} \div 10^{26}$	$0.3 \cdot 10^{-3} \div 1$	Impacts the Earth
The Tunguska event	$5 \cdot 10^{16}$	$5 \cdot 10^{16}$	1	—
Lightning	$10^{10} \div 10^{12}$	$10^{10} \div 10^{12}$	1	—
Global winds	10^{20}	10^{15}	10^5	During 24 hours
Cyclone	$10^{19} \div 10^{21}$	$2 \cdot 10^{13} \div 2 \cdot 10^{15}$	$5 \cdot 10^5$	—
Hurricane	$10^{18} \div 10^{20}$	$10^{13} \div 10^{15}$	10^5	During 24 hours
Tornado	$10^{11} \div 10^{13}$	$10^8 \div 10^{10}$	10^3	—
Volcano	$10^{20} \div 10^{21}$	$10^{15} \div 10^{19}$	$10^2 \div 10^5$	—
Earthquake	$10^{19} \div 10^{21}$	$10^{17} \div 10^{18}$	$10^2 \div 10^3$	—
Tsunami	$10^{18} \div 10^{20}$	$10^{16} \div 10^{19}$	$10 \div 10^2$	—
Forest fire	$10^{18} \div 10^{19}$	$10^{12} \div 10^{14}$	$10^5 \div 10^6$	1000 km^2 area
Heat flux from the Earth's interior	$3 \cdot 10^{18}$	$3 \cdot 10^{13}$	10^5	During 24 hours

The energetics of the fields of seismic origin is high, as the data in Table 8 show.

Earthquakes are the cause of both the secondary effects arising in the EAIM system and the manifestation of the coupling in the ionosphere-magnetosphere-atmosphere-ionosphere system recurring under the influence of energetic particles precipitating from the radiation belts, as the data in Table 9 illustrate [1, 4].

3.3. Meteorological Processes

General Information. A conjecture that powerful meteorological processes can influence the upper atmosphere has circulated for a long time; however, the convincing evidence has appeared only recently. The important role is played by cyclones, specifically, by extratropical cyclones that occur almost continuously, and this means that their impact on the upper atmosphere may be regular. The tropical cyclone is distinct from that extratropical in a nonlinear coupling between the ocean and the troposphere.

Most likely, the geomagnetic storm and tropical cyclone occurrences show a statistical correlation.

The tropical cyclone turns out to generate bipolar changes of 10 to 20 mV/m in the electric field. Satellite measurements show that the duration of this process is approximately $2 \div 3$ min with horizontal scales of $(1 \div 1.5) \cdot 10^3$ km.

Chernogor [3, 10] has developed the basis for hydrodynamic, thermodynamic, and electromagnetic field models of the tropical cyclone (Tables 10–12).

The tropical cyclone, like other meteorological processes, is formed as a result of coupling among the constituents in the atmosphere-ocean-land (AOL) subsystem. This subsystem has an inherent property of self-excitation. The initial eddy can be induced by a few mechanisms, such as an air current disturbance by a sharp discontinuity in the mainland landform, a meteorological front, or cumulus cloud development. The initial eddy

Table 4. *Parameters of anthropogenic sources in the EAIM system*

Source	Energy (J)	Power(W)	Impact duration (s)	Comments
Nuclear explosions: single all ammunition anti-asteroid perspective	 $4\cdot10^{17}$ $4\cdot10^{19}$ $4\cdot10^{18}\div4\cdot10^{21}$	 $4\cdot10^{24}$ $4\cdot10^{15}\div4\cdot10^{16}$ $4\cdot10^{25}\div4\cdot10^{28}$	 10^{-7} $10^{3}\div10^{4}$ 10^{-7}	 Equivalent of 100 Mt Global nuclear conflict
Large surface explosion	$10^{11}\div10^{12}$	$10^{14}\div10^{15}$	10^{-3}	Mass of $25\div250$ t
Nuclear plant accident	10^{18}	$10^{13}\div10^{14}$	$10^{4}\div10^{5}$	Fuel mass of 100 t
Large rocket explosion	10^{13}	$10^{12}\div10^{14}$	$0.1\div10$	Fuel mass of 1000 t
Rocket launch: large expected	 10^{13} $10^{14}\div10^{15}$	 $10^{10}\div10^{11}$ $10^{11}\div10^{13}$	 $10^{2}\div10^{3}$ $10^{2}\div10^{3}$	 Same as above Fuel mass of $10^{4}\div10^{5}$ t
Orbital maneuvering system engine burn in space	$10^{7}\div10^{9}$	$10^{7}\div10^{8}$	$1\div10$	—
Nuclear power system for space probe	10^{14}	10^{9}	10^{5}	During 24 hours
Spacecraft descent: large expected	 $10^{12}\div10^{13}$ $10^{14}\div10^{15}$	 $10^{9}\div10^{11}$ $10^{11}\div10^{13}$	 $10^{2}\div10^{3}$ $10^{2}\div10^{3}$	 Mass: 100 t $10^{3}\div10^{4}$ t
Power transmission line	10^{15}	10^{10}	10^{5}	During 24 hours
Radio system emissions	10^{12}	10^{7}	10^{5}	Same as above
Meteotron	$10^{12}\div10^{15}$	$10^{9}\div10^{10}$	$10^{3}\div10^{5}$	—
Power plant	$10^{14}\div10^{15}$	$10^{9}\div10^{10}$	10^{5}	Same as above
Power plants worldwide	$2\cdot10^{17}$	$2\cdot10^{12}$	10^{5}	Same as above
Global energy consumption	$2\cdot10^{18}$	$2\cdot10^{13}$	10^{5}	Same as above

Table 5. *Geospace storm energetics*

Geospace region	Energy (J)	Power (W)	Duration (s)	Relative variations in energy	Comments
Magnetosphere	10^{16}	10^{12}	10^{4}	10^{-2}	Magnetic field energy
	$10^{8}\div10^{10}$	$10^{4}\div10^{6}$	$10^{4}\div10^{5}$	$10^{2}\div10^{4}$	Electric field energy
Ionosphere	10^{12}	10^{8}	10^{4}	±1	Thermal energy
	$10^{5}\div10^{7}$	$10\div10^{3}$	$10^{4}\div10^{5}$	$10^{2}\div10^{4}$	Electric field energy
Thermosphere	$10^{15}\div10^{17}$	$10^{11}\div10^{13}$	$10^{4}\div10^{5}$	$10^{-3}\div10^{-1}$	Thermal energy

Table 6. *Magnetic storm parameter estimates*

K index	ΔB (nT)	Δt (h)	ΔE_m (J)	P_m (W)	Qualitative disturbance/storm description
0	<3	1	$(1\div1.5)\cdot10^{14}$	$(2.8\div4.2)\cdot10^{10}$	Ultra weak disturbance
1	$3\div5$	$1\div2$	$(1.5\div2.5)\cdot10^{14}$	$(2.1\div7)\cdot10^{10}$	Extremely weak disturbance
2	$5\div10$	$1\div2$	$(2.5\div5)\cdot10^{14}$	$(3.5\div14)\cdot10^{10}$	Very weak disturbance
3	$10\div20$	$1\div2$	$(0.5\div1)\cdot10^{15}$	$(0.7\div2.8)\cdot10^{11}$	Weak storm
4	$20\div40$	$1\div2$	$(1\div2)\cdot10^{15}$	$(1.4\div5.6)\cdot10^{11}$	Relatively moderate storm
5	$40\div70$	$2\div3$	$(2\div5)\cdot10^{15}$	$(1.9\div4.9)\cdot10^{11}$	Moderate storm
6	$70\div120$	$3\div4$	$(3.5\div6)\cdot10^{15}$	$(2.5\div5.6)\cdot10^{11}$	Strong storm
7	$120\div200$	$4\div5$	$(0.6\div1)\cdot10^{16}$	$(3.4\div7.7)\cdot10^{11}$	Very strong storm
8	$200\div330$	$5\div10$	$(1\div1.7)\cdot10^{16}$	$(2.8\div9.5)\cdot10^{11}$	Ultra strong storm
9	$330\div500$	$6\div12$	$(1.7\div2.5)\cdot10^{16}$	$(0.4\div1.2)\cdot10^{12}$	Super strong storm

Table 7. *The characterization of geospace storm components: a magnetic storm (MS), an ionospheric storm (IS), an atmospheric (thermospheric) storm (AS), an electrical storm (ES), the main ionospheric trough (MIT), a traveling ionospheric disturbance (TID). Here, N_mF_2 is the F_2-layer peak electron density*

Storm intensity	Examples	Ionospheric storm effects	Causes	Mechanism
Intensive MS Intensive IS Intensive AS Intensive ES	September 25, 1998, May 29-30, 2003, and November 7-10, 2004 storms	A decrease in *NmF*2 by a factor of $4\div7$ times. Nighttime plasma heating up to $2400\div3200$ K. An uplifting of the F2 region by $100\div300$ km. A decrease in the relative hydrogen ion density $N(H^+)/Ne$ down to 10 times with the subsequent recovery. The effects of magnetospheric electric fields penetrating to middle latitudes.	The auroral oval, MIT, light ion trough, and auroral hot spot expansion to middle latitudes, the emptying of magnetic flux tubes. Magnetospheric substorms.	Reconnection between interplanetary and magnetospheric field lines. Deformation of the magnetosphere. Energetic particle precipitation from the magnetosphere.
Moderate MS Intensive IS Intensive AS Intensive ES	March 20-21, 2003 storm	A decrease in *NmF*2 down to 5 times, associated with an increase in T_e during sunlit hours up to $2700\div3300$ K in the $300\div500$ km altitude range. An uplifting of the F-layer peak altitude more than by 100 km during the night. The effects of TIDs and magnetospheric electric fields penetrating to middle latitudes.	A change in the storm phase due to the destabilizing electric field pulse associated with the change in the sign of the IMF E_y component from east to west and with the TIDs generated by magnetospheric substorms.	Magnetospheric substorms associated with the generation of TIDs and nonstationary disturbances in the magnetospheric electric fields.
Intensive MS Moderate IS Moderate AS Weak ES	April 17, 2002 storm	An increase in *NmF*2 of 15 %. An uplifting of the F2 region by ~50 km. The plasma temperature does not change.	The rearrangement of the global thermospheric circulation and neutral constituent redistribution due to high latitude atmospheric heating.	The transformation of a negative IS at high latitudes into the positive phase in the mid-latitude daytime sector.

Table 8. *Enegetics charecterizing the fields of seismic origin*

Field	Energy (J)	Power (W)	Duration (s)	Comments
Electromagnetic: $f \le 10$ Hz	$10^{10} \div 10^{11}$	10^{8}	$10^{2} \div 10^{3}$	Reach the ionosphere and magnetosphere
$f = 10^{3} \div 10^{4}$ Hz	$10^{13} \div 10^{14}$	10^{11}	$10^{2} \div 10^{3}$	Same as above
$f = 10^{5} \div 10^{6}$ Hz	$10^{15} \div 10^{16}$	10^{13}	$10^{2} \div 10^{3}$	Rapidly decay in the lithosphere
Electric	10^{9}	$10^{4} \div 10^{6}$	$10^{3} \div 10^{5}$	Reach the ionosphere
Magnetic	10^{10}	10^{8}	10^{2}	Same as above
Infrasound	$10^{15} \div 10^{16}$	$10^{13} \div 10^{14}$	10^{2}	Reach ~300 km altitude
AGW	$10^{15} \div 10^{16}$	$10^{11} \div 10^{12}$	$10^{3} \div 10^{4}$	Same as above

Table 9. *The parameters of precipitating energetic particle fluxes and the produced ionization as estimated from MF radar electron density measurements*

Event	Date	Particles	Altitude (km)	N (m^{-3})	ΔN (m^{-3})	q ($m^{-3} \cdot s^{-1}$)	Δq ($m^{-3} \cdot s^{-1}$)	Π_p (W/m^2)	Π ($m^{-2} \cdot s^{-1}$)	ε (keV)
Magnetic storm	June 15, 1983	Electrons (protons)	$55 \div 60$	10^{8}	$3 \cdot 10^{8}$	10^{5}	$15 \cdot 10^{5}$	$1.8 \cdot 10^{-6}$	$2.3 \cdot 10^{7}$ ($7.8 \cdot 10^{5}$)	500 (15000)
Magnetic storm	May 15, 1997	Electrons	84	$1.2 \cdot 10^{9}$	$0.5 \cdot 10^{9}$	$1.4 \cdot 10^{7}$	$1.5 \cdot 10^{7}$	$1.5 \cdot 10^{-6}$	$3.8 \cdot 10^{8}$	60
Proton flare	February 25, 1991	Electrons (protons)	72.5	10^{9}	$5 \cdot 10^{9}$	10^{7}	$35 \cdot 10^{7}$	$3.5 \cdot 10^{-5}$	$1.6 \cdot 10^{9}$ ($1.2 \cdot 10^{7}$)	150 (20000)
Dusk terminator	May 24, 1997	Electrons	80	10^{9}	10^{9}	10^{7}	$3 \cdot 10^{7}$	$3.4 \cdot 10^{-6}$	$2.7 \cdot 10^{8}$	80
Dawn terminator	May 25, 1997	Electrons	80	$8 \cdot 10^{8}$	$6 \cdot 10^{8}$	$6.4 \cdot 10^{6}$	$1.3 \cdot 10^{7}$	$2.2 \cdot 10^{-6}$	$1.7 \cdot 10^{8}$	80
Midnight	May 25, 1997	Electrons	90	—	$3 \cdot 10^{8}$	—	$3 \cdot 10^{5}$	$3 \cdot 10^{-8}$	$5 \cdot 10^{6}$	40
Solar eclipse	August 11, 1999	Electrons	84	$3 \cdot 10^{8}$	$5 \cdot 10^{8}$	$9 \cdot 10^{5}$	$55 \cdot 10^{5}$	$3.1 \cdot 10^{-7}$	$3.2 \cdot 10^{7}$	60
Earthquake	August 24, 1999	Electrons	84	$5 \cdot 10^{8}$	$4 \cdot 10^{8}$	$2.5 \cdot 10^{6}$	$5.6 \cdot 10^{6}$	$6.3 \cdot 10^{-7}$	$6.6 \cdot 10^{7}$	60
Rocket launch	May 15, 1987	Electrons	80	10^{9}	10^{9}	$3 \cdot 10^{6}$	$9 \cdot 10^{6}$	10^{-6}	$2 \cdot 10^{8}$	80
High-power HF radio emissions	March 1, 1991	Electrons	88	$4 \cdot 10^{9}$	$3 \cdot 10^{9}$	$1.3 \cdot 10^{7}$	$2.7 \cdot 10^{7}$	$2.7 \cdot 10^{-6}$	$4.5 \cdot 10^{8}$	40

Here, N is the electron density, ΔN is an enhancement in the electron density, q is the electron-ion production rate, Δq is an enhancement in the electron-ion production rate, Π_p is a precipitation energy rate, Π is an energetic particle flux, ε is precipitating particle energy.

Table 10. *Hydrodynamic model for the tropical cyclone*

υ_0 (m/s)	u_0 (m/s)	V_0 (m/s)	ω_0 (cm/s)	υ_1 (m/s)	r_0 (km)	R_0 (km)	m (10^{15} kg)	E_k (10^{18} J)	$\Delta p(r_0)$ (hPa)
15	4.8	15.8	1.8	3	10	400	5	$5.6\cdot10^{-2}$	7.7
20	6.4	21	4.8	4	10	425	5.7	$1.1\cdot10^{-1}$	13.6
25	8	26.3	10.8	5	11	450	6.4	$1.9\cdot10^{-1}$	21.3
30	9.6	31.5	19.2	6	11	475	7.1	$3.2\cdot10^{-1}$	30.6
35	11.2	36.8	28	7	12	500	7.9	$4.8\cdot10^{-1}$	41.7
40	12.8	42	36	8	13	530	8.8	$7\cdot10^{-1}$	54.4
50	16	52.5	42	10	14	570	10.2	1.3	85
60	19.2	63	47	12	15	610	11.7	2.1	122
70	22.4	73.5	52	14	16	650	13.3	3.3	167
80	25.6	84	53	16	18	700	15.4	4.9	218
90	28.8	94.5	53	18	20	750	17.7	7	275

Here, υ_0 is the tangential component of the air velocity at the tropical cyclone internal boundary of radius r_0, u_0 is the radial speed, V_0 is the horizontal velocity component, ω_0 the vertical velocity component at a range of r_0 from the cyclone center, υ_1 is the forward speed, r_0 is the inner boundary radius, R_0 is the outer boundary radius, m is the moving air mass, E_k is the tropical cyclone kinetic energy, $\Delta p(r_0)$ is an air pressure deficit.

Table 11. *Thermodynamic model for the tropical cyclone*

υ_0 (m/s)	$\overline{\Delta T_1}$ (K)	h_1 (m)	P_{T1} (10^{14} W)	P_f (10^{14} W)	P_f/P_{T1} (%)	τ_s (24 h)	P_c (10^{14} W)	Δt_2 (°C)	P_{T2} (10^{14} W)
15	1	20	$2.6\cdot10^{-1}$	$1.7\cdot10^{-3}$	3.4	6.6	$2.5\cdot10^{-2}$	12.1	$3.3\cdot10^{-2}$
20	1.3	30	0.8	$4.6\cdot10^{-3}$	3.6	4.2	$7.2\cdot10^{-2}$	12.6	$9.6\cdot10^{-2}$
25	1.5	50	1.8	10^{-2}	3.4	4	$1.8\cdot10^{-1}$	12.2	$2.4\cdot10^{-1}$
30	2	60	3.7	$1.9\cdot10^{-2}$	3.4	3.4	$3.6\cdot10^{-1}$	12.7	0.5
35	2.1	70	5.6	$3.4\cdot10^{-2}$	3.4	2.8	$5.6\cdot10^{-1}$	12.5	$7.5\cdot10^{-1}$
40	2.4	80	8.4	$5.6\cdot10^{-2}$	2.4	2.4	$8.5\cdot10^{-1}$	12.2	1.1
50	2.4	80	9.6	$1.3\cdot10^{-1}$	3	2	1.1	12.2	1.6
60	2.4	80	15.2	$2.5\cdot10^{-1}$	2.8	1.6	1.5	12.2	2
70	2.5	80	19.2	$4.6\cdot10^{-1}$	2.8	1.4	1.9	12.2	2.5
80	2.5	80	23.4	$7.9\cdot10^{-1}$	3	1.1	2.3	11.8	3.7
90	2.5	85	30.1	1.3	3.2	1	2.7	11.6	5

Here, υ_0 is the tangential velocity component, $\overline{\Delta T_1}$ is the water layer cooling, h_1 is the cooled water layer thickness, P_{T1} is the thermal power lost by the ocean, P_f is the power transferred by the cyclone to the ocean, P_f/P_{T1} is the energy transfer coefficient, τ_s is the characteristic time constant for cyclone development, P_c is the power of the latent heat yield, Δt_2 is an increase in the air temperature, P_{T2} is the power needed for water evaporation.

Table 12. *Electrical and magnetic parameters of the tropical cyclone*

Q (C/m^3)	10^{-10}	10^{-9}	10^{-8}	10^{-7}	10^{-6}	10^{-5}	10^{-4}
w_0 (m/s)	$3\cdot10^{-2}$	$4\cdot10^{-2}$	$5\cdot10^{-2}$	0.1	0.2	0.3	0.5
j_a (A/m^2)	$3\cdot10^{-12}$	$4\cdot10^{-11}$	$5\cdot10^{-10}$	10^{-8}	$2\cdot10^{-7}$	$3\cdot10^{-6}$	$5\cdot10^{-4}$
$\dot{Q}$ (A/m^3)	$3\cdot10^{-16}$	$4\cdot10^{-15}$	$5\cdot10^{-14}$	10^{-12}	$2\cdot10^{-11}$	$3\cdot10^{-10}$	$5\cdot10^{-8}$
E_e (V/m)	10^5	$2\cdot10^5$	$4\cdot10^5$	$6\cdot10^5$	$8\cdot10^5$	10^6	$2\cdot10^6$
F_e (N/m^3)	10^{-5}	$2\cdot10^{-4}$	$4\cdot10^{-3}$	$6\cdot10^{-2}$	0.8	10	$2\cdot10^2$
F_p (N/m^3)	0.1	0.3	0.6	0.8	1.1	1.2	1.4
F_k (N/m^3)	$2\cdot10^{-3}$	$4\cdot10^{-3}$	$7\cdot10^{-3}$	$8\cdot10^{-3}$	$9\cdot10^{-3}$	10^{-2}	$1.2\cdot10^{-2}$
F_c (N/m^3)	$3\cdot10^{-2}$	0.1	0.2	0.3	0.4	0.5	0.5
υ_0 (m/s)	15	30	50	60	70	80	90
r_0 (km)	10	11	14	15	16	18	20
$\Delta p(r_0)$ (kPa)	0.8	3	9	12	17	22	28
R_0 (km)	400	450	570	610	650	700	750
$\Delta B(R_0)$ (nT)	$8\cdot10^{-4}$	$1.1\cdot10^{-2}$	0.2	3.8	82	$1.3\cdot10^3$	$2.4\cdot10^4$

Here, E_e is the electric field intensity in the cloud, $F_e = QE_e$ is the electric force per unit volume, $F_p = \Delta p(r_0)/r_0$ is the pressure-gradient force, $F_k = 2w\upsilon_0\rho$ is the Coriolis force per unit volume, $F_c = \rho\upsilon_0^2/2$ is the centrifugal force per unit volume, Q is the electric charge density, w_0 is the cyclone vertical velocity component, j_a is the atmospheric electric current density, $\dot{Q}$ is the charge separation rate, υ_0 is the tangential component of the air velocity at the tropical cyclone internal boundary, r_0 is the radius of the tropical cyclone internal boundary, $\Delta p(r_0)$ is an air pressure deficit, R_0 is the outer radius of the cyclone, $\Delta B(R_0)$ is the changes in the magnetic field at a range of R_0.

is further strengthened when cool air runs over the warm oceanic surface, which temperature is higher than the critical value of $t_C \approx 26.5$ °C, and the oceanic upper layer of $10 \div 100$ m thickness transfers its heat to the evolving eddy. The heat causes evaporation of the oceanic water, warms the air, and increases the eddy kinetic energy. When the water temperature, t_1, becomes less than the air temperature, the air begins to warm the oceanic surface layer, and thus a nonlinear decaying oscillatory (in some cases, aperiodic) process arises.

The tropical cyclone speed increases owing to the heat transferred from the oceanic surface layer water, and it decreases as a result of the air friction against the oceanic surface. It is important that the frictional force is proportional to the eddy air velocity squared, υ^2.

To compensate for a horizontal divergence of the flow in the surface layer caused by winds, the upwelling of subsurface cold water occurs. The sea surface temperature, t_f, is determined by solar heating, and usually $t_f = 27 \div 30$ °C when tropical cyclones occur. The layer water-cooling rate is controlled by the eddy frictional force, which is proportional to υ^2. Thus, the heat balance equation for the oceanic surface layer and the balance equation for the eddy kinetic energy are nonlinear [3, 10]. This means that both the AOL system and the processes acting in it are nonlinear.

The temperature in the cyclone at the air-earth boundary increases by $\Delta T \approx 10$ K.

AGW Channel. The heating and eddy motion occurring in the tropical cyclone generate internal gravity waves that break in the upper atmosphere and heat it. The predominant components in the internal gravity wave spectrum occur at two frequencies, Ω_1 and Ω_2, one is the Brunt-Vaisala frequency $\Omega_1 = \omega_B$ and the other is $\Omega_2 \approx 10V_0/R_0$ where V_0 is the tangential component of the air velocity at the tropical cyclone internal boundary of radius r_0. In addition, the oceanic waves

associated with the tropical cyclone are a powerful source of infrasound. The maximum in the infrasound spectrum occurs at a frequency of $\Omega_2 = 2(2)^{1/2}\, g/(3\pi V_0)$ where $g \approx 9.8$ m/s^2. The calculations of IGW and infrasound parameters are presented in Tables 13 and 14.

As the IGW propagate upwards, their effect on the atmosphere evolves. At altitudes of less than $z < z_0 \sim 100$ km, they only modulate neutral air and plasma parameters, while at $z > z_0$ nonlinear dissipation adds, and consequently neutral air heating occurs. Moreover, the air temperature turns out to be modulated at the double (in the first approximation) frequency. The additional heating and modulation in turn cause changes and modulation in such a plasma parameter as the conductivity tensor (depending on the temperature), and consequently variations in the dynamo electric current arising owing to the neutral air drag on the charge particle. The $10 \div 100$ % variation in the upper atmospheric temperature results in tens of percent disturbances in the ionospheric conductivity tensor components, and consequently in the integral ionospheric current giving rise to the geomagnetic effect of internal gravity waves. Chernogor [3, 10] has obtained the following relation for estimating the amplitude of the geomagnetic field disturbance at a frequency of 2Ω:

$$\Delta B_\Omega \approx \frac{\theta_m}{2\Omega\tau_T}\mu_0 I_0$$

where μ_0 is the permeability of free space. During sunlit hours, the amplitude of the disturbance lies in the range $\Delta B_\Omega \approx 1.3 \div 13$ nT, if $\theta_m = \Delta T/T = 0.1 \div 1$, $\Omega = 10^{-3}$ s^{-1}, the gas relaxation time constant $\tau_T = 10^4$ s, and the undisturbed integral current $I_0 = 0.2$ A/m. Measurements show the magnitudes of ΔB_Ω close to these values.

The nighttime values of I_0 and ΔB_Ω are an order of magnitude smaller.

The physical mechanism for the impact of infrasound on the upper atmosphere is similar to that for the IGW effects. The upper atmospheric responses to these impacts are also similar, and the differences lie in the values of the predominant periods in the spectrum of geomagnetic field variations. The infrasound effects are associated with geomagnetic pulsation enhancements in the unity to tenths second period range. The effect is clearly pronounced

Table 13. *Parameters of IGW launched by the tropical cyclone*

υ_0(m/s)	$\delta p_m(R_0)$ (Pa)	$\upsilon_w(R_0)$ (mm/s)	Π_r (W/m^2)	P_r (TW)	S_r (10^{12} m^2)
15	$1.6\cdot10^{-2}$	$3.6\cdot10^{-2}$	$5.7\cdot10^{-7}$	$2.9\cdot10^{-7}$	0.5
20	$5.1\cdot10^{-2}$	$1.2\cdot10^{-1}$	$5.9\cdot10^{-6}$	$3.4\cdot10^{-6}$	0.57
25	$1.3\cdot10^{-1}$	$2.9\cdot10^{-1}$	$3.8\cdot10^{-5}$	$2.4\cdot10^{-5}$	0.64
30	$2.7\cdot10^{-1}$	$6.1\cdot10^{-1}$	$1.6\cdot10^{-4}$	$1.1\cdot10^{-4}$	0.71
35	0.5	1.1	$5.7\cdot10^{-4}$	$4.5\cdot10^{-4}$	0.79
40	0.8	1.9	$1.6\cdot10^{-3}$	$1.4\cdot10^{-3}$	0.88
50	2.1	4.7	$9.5\cdot10^{-3}$	$9.5\cdot10^{-3}$	1
60	4.3	9.7	$4\cdot10^{-2}$	$4.5\cdot10^{-2}$	1.12
70	7.7	17.4	$1.3\cdot10^{-1}$	$1.7\cdot10^{-1}$	1.33
80	12.9	29.2	$3.8\cdot10^{-1}$	$5.8\cdot10^{-1}$	1.54
90	19.6	44.3	0.9	1.6	1.77

Here, υ_θ is the tangential velocity component, $\delta p_m(R_0)$ is the rms amplitude of the pressure in the IGW, $\upsilon_w(R_0)$ is the particle velocity in the IGW, Π_r is the energy flux density in the IGW, P_r is the power of IGW emission, S_r is the surface area of IGW emission.

Table 14. *The main parameters of acoustic emissions from oceanic waves*

v_0 (m/s)	f_m (mHz)	T_m (s)	Π_{a0} (W/m^2)	δp_a (Pa)	v_w (m/s)	S_a (10^9 m^2)	P_a (W)
10	147	6.8	$3.7\cdot10^{-7}$	$1.3\cdot10^{-2}$	$2.9\cdot10^{-5}$	0.7	$2.6\cdot10^{2}$
15	98	10.2	$9.2\cdot10^{-6}$	$6.4\cdot10^{-2}$	$1.4\cdot10^{-4}$	0.7	$6.5\cdot10^{3}$
20	74	13.6	$9.2\cdot10^{-5}$	0.2	$4.5\cdot10^{-4}$	0.7	$6.5\cdot10^{4}$
25	59	17	$5.5\cdot10^{-4}$	0.5	$1.1\cdot10^{-3}$	0.85	$4.7\cdot10^{5}$
30	49	20.4	$2.4\cdot10^{-3}$	1	$2.3\cdot10^{-3}$	0.85	$2\cdot10^{6}$
35	42	23.8	$8.1\cdot10^{-3}$	1.9	$4.3\cdot10^{-3}$	1	$8.1\cdot10^{6}$
40	37	27.2	$2.4\cdot10^{-2}$	3.3	$7.5\cdot10^{-3}$	1.2	$2.9\cdot10^{7}$
50	29	34	0.14	7.9	$1.8\cdot10^{-2}$	1.4	$2\cdot10^{8}$
60	25	40.8	0.6	16.3	$3.7\cdot10^{-2}$	1.6	$9.6\cdot10^{8}$
70	21	47.6	2.1	30.4	$6.9\cdot10^{-2}$	1.8	$3.8\cdot10^{9}$
80	18	54.4	6	51.4	0.12	2.3	$1.4\cdot10^{10}$
90	16	61.2	15.5	82.7	0.19	2.8	$4.3\cdot10^{10}$

Here, v_0 is the tangential velocity component, f_m is the maximum infrasound emission frequency, T_m is the maximum infrasound emission period, Π_{a0} is the infrasound energy flux density, δp_a is the infrasound wave amplitude, v_w is the particle velocity in the wave, S_a is the surface area of the acoustic source, P_a is the power of acoustic emission.

only at the principal infrasound frequencies of $\Omega \approx 0.1 \div 1.0$ s^{-1} with $\Delta B \sim 0.1 \div 1$ nT in the daytime.

Electromagnetic Emission Generation. Tropical Cyclone Impacts on the Magnetosphere and the Radiation Belts. The tropical cyclone evolution is generally accompanied by thunderstorms, thus resulting in generation of electromagnetic emissions in a wide range of frequencies ($\Delta f \le 100$ kHz). Rocket and satellite measurements support this concept. The energy and power of the strongest lightning discharges attain values of 10 GJ and 10 GW, respectively. During a tropical cyclone lifetime, the total number of lightning discharges reaches $10^3 \div 10^4$, which total energy and power yield attains 10^2 TJ and 10^2 TW, respectively. Approximately 10^{-3} of the lightning energy is converted into the acoustic disturbances and $10^{-4} \div 10^{-3}$ into the electromagnetic disturbances, and consequently a total of 10^4 lightning discharges amounts to approximately 100 GJ acoustic energy and $10 \div 100$ GJ electromagnetic energy. For a tropical cyclone lifetime of 6 days, the average acoustic emission power amounts to 200 kW and electromagnetic to $20 \div 200$ kW.

The acoustic and electromagnetic energy fluxes reaching the upper atmosphere appreciably change its parameters in the $\sim 50 \div 100$ km altitude range. Moreover, the VLF emissions propagating along geomagnetic field lines into the magnetosphere filled with the energetic particles drive the electromagnetic electron and ion cyclotron instabilities resulting in pitch angle scattering of the energetic particles via wave-particle interaction and consequently in the magnetospheric energetic particle precipitation into the upper atmosphere. The equations governing VLF or Alfven emission flux variations and the total content of energetic particles in the geomagnetic flux tube containing the wave source are nonlinear [1, 3].

The VLF radio waves cause precipitation of the energetic electrons, and the Alfven waves cause precipitation of the energetic ions, both of which produce additional ionization in the

upper atmosphere and modulate the atmospheric electric current flow, which, in turn, produce low-frequency emissions. Consequently, the above-mentioned secondary processes occur. In this way, cyclones affect the magnetosphere and the radiation belts, and the magnetosphere and the radiation belts produce feedback on the lower regions of the near-Earth space environment.

Quasi-Steady Electric Field Generation. Impacts on the Magnetosphere and the Radiation Belts. The marine aerosol plays a key role in the generation of the quasi-steady electric field. A few mechanisms are suggested for this aerosol formation. The largest aerosol ($d_a > 1$ μm in diameter) originate from droplets spraying and drying at the wind velocity of $V > 7$ m/s and from water trickles ejected from breaking bubbles. Under quiet conditions, the aerosol number n_a and mass ρ_a densities do not exceed $5 \cdot 10^4$ m^{-3} and $5 \cdot 10^{-11}$ kg/m^3, respectively. The smaller aerosol ($d_a < 1$ μm in diameter) is mainly formed at the moment when the envelope of the surfacing bubble with an excessive vapor pressure is bursting. Another way of aerosol forming in this diameter range is the shrinking of the broken bubble envelope. The maximum in the size distribution function for this aerosol occurs at $d_a > 0.1$ μm, and $n_a \approx (3 \div 5) \cdot 10^8$ m^{-3} and $\rho_a \approx (3 \div 5) \cdot 10^{-10}$ kg/m^3 under quiet conditions. The strong wind within the cyclone facilitates the more intensive formation of aerosol, its electrification, charge separation, etc. When $V = 35$ m/s, the $n_a \approx 10^{11}$ m^{-3} and $\rho_a \approx 10^{-6}$ kg/m^3 values are attained.

In the developed cyclone, the aerosol formation is appreciably activated.

The principal mechanism for aerosol formation within the tropical cyclone is droplet spraying. The effect of the ascending air currents in the cyclone is to transport the positively charged aerosols upwards, while the larger drops charged negatively move downward. As a result, the atmospheric electric current density, j_a, significantly increases, and an increase in precipitation results in a significant increase in j_a. During heavy showers usually associated with tropical cyclones, the j_a value can attain 10^{-8} A/m^2 or even 10^{-7} A/m^2, while under quiet conditions $j_{a0} \approx 3 \cdot 10^{-12}$ A/m^2. At the wind vertical component of w, the electric charge density is given by $Q = j_a / w = 1.7 \cdot 10^{-7}$ C/m^3 and the charge separation rate $\dot{Q} = j_a / H_a \approx 10^{-11}$ A/m^3 where the dot over the letter designates the derivative taken with respect to time, and H_a is a cloud thickness usually equal to 10 km. These values are the upper bound, while the more probable values are $j_{a0} \approx 3 \cdot 10^{-9} \div 3 \cdot 10^{-8}$ A/m^2 and $\dot{Q} = j_a / H_a \approx 10^{-13} \div 10^{-12}$ A/m^3. It is important that $j_a / j_{a0} \approx 10^3 \div 10^4$ even in the latter case.

The appearance of the strong electric current results in the generation of a quasi-steady electric field in the upper atmosphere, ionosphere, and the magnetosphere [3, 10]. To evaluate the electric field generated by the cyclone in the ionosphere, the following relation has been obtained:

$$E_i = E_0 \frac{\sigma_0}{\sigma_i} \frac{j_a}{j_0}$$

where $\sigma_i \approx 10^{-6}$ S/m is the conductance of the plasma at the ionospheric lower bound, $E_0 \approx 150$ V/m is the electric field intensity at the water surface, and σ_0 is the air conductance at the water surface. Inserting the j_a estimate obtained above into this relation yields $E_i \approx 3 \div 30$ mV/m, which exceeds the background electric field in the ionosphere by $1 \div 2$ orders of magnitude. Besides, the maximum in this field occurs not strictly above the cyclone, but some distance away from it. The shift occurs because this disturbance maps from the dynamo region altitudes ($z \approx 100 \div 150$ km) to higher altitudes along magnetic field lines, and its value attains $600 \div 800$ km, which is of the same order of magnitude as cyclone dimensions [3, 10].

This electric field mapping into the magnetosphere along magnetic field lines occurs without significant attenuation and, under some conditions, acts to decrease the charged particle transverse energy by $\varepsilon_\perp = eE_i L_\perp$ where $L_\perp$ is the horizontal scale of the electric field disturbance. Set-

ting $L_\perp = 2R_0 \approx 1000$ km gives $\varepsilon_\perp \approx 5 \div 50$ keV. These $\varepsilon_\perp$ values are sufficient to cause particle pitch angle scattering, the precipitation of a fraction of radiation belt particles into the upper atmosphere, and the onset of the secondary processes mentioned above.

Enhancements in the atmospheric electric currents over the cyclone act to produce variations in the geomagnetic field. Estimates of the changes in the magnetic field at a range of R can be provided by the well-known relation

$$\Delta B = \mu_0 \frac{I_a}{2\pi R}.$$

Here, $I_a = j_a S_0$ where $S_0 = \pi R_0^2$, R_0 is the outer radius of the cyclone. The $\Delta B(R_0)$ estimates are presented in Table 12 where E_e is the electric field in the cloud, $F_e = QE_e$ is the electric force per unit volume, $F_p = \Delta p(r_0)/r_0$ is the pressure-gradient force, $F_k = 2\omega v_0 \rho$ is the Coriolis force per unit volume, $F_c = \rho v_0^2/2$ is the centrifugal force per unit volume, ω_0 is the cyclone vertical velocity component at a range of r_0 from its center, j_a is the atmospheric electric current density, $\dot{Q}$ is the rate of change of charge per unit volume in the cyclone.

3.4. Solar Eclipses

Solar eclipses also belong to high-energy processes occurring in the atmosphere and geospace and acting to reconstruct EAIM subsystems coupling [11].

3.5. Subsystem Coupling

The subsystems in the EAIM system are strongly coupled via (1) waves of various origin, which modulate the parameters of the medium and transform one into the other, (2) quasi-steady electromagnetic fields, (3) particle fluxes from the ionosphere into the plasmasphere and vice versa, (4) energetic particles precipitating from the magnetosphere (see Table 9).

The wave disturbances play a prominent role in the system paradigm for the investigation of the EAIM system [12-17]. The wave disturbances not only transport energy and momentum, but they also indicate their state and variations in space (and tropospheric) weather.

The list of wave types and their parameters are presented in Table 15 [1, 4].

Particle Precipitation. Our theoretical and experimental results indicate that energetic electron precipitation at middle latitudes accompany the majority of highly variable processes occurring in the EAIM system [1-4, 12, 18], and the electron fluxes attain values of $10^7 \div 10^9$ $m^{-2}s^{-1}$. The mechanisms for the precipitation of particles have been validated, and they include the deceleration of the energetic electrons in an ionospheric-magnetospheric quasi-static electric field and the transfer of their energy to VLF noise.

Active Experiments proved to be a convenient way of studying both the EAIM system as a whole and its subsystem coupling. They permit the choice to be made of the energy yield, the location, and the time of the energy release, which is impossible to achieve when studying the naturally occurring processes in the EAIM system [1-4, 13, 16, 17, 19, 20].

Military Operations are accompanied by significant energy yields, similar to those during active experiments [4, 21].

The modern regional wars and conflicts, being non-nuclear, employ ammunition powerful enough to be an important tool for remotely studying the near-Earth environment [4, 21], and during these wars impacts on the EAIM system become many times greater. Wars are usually waged on land and at the air-earth boundary and can impact the lithosphere, the entire atmosphere, and even geospace, as well as the geoelectric and geomagnetic fields.

Wars produce atmospheric pollution of many types. These include dust, smoke, and disruption in the thermal and dynamic regimes in the underlying surface-troposphere system, as well as hazardous ecological consequences, such as carbon hydrocarbon ($\sim 10 \div 100$ % of the background atmospheric content) and the acids HCl, H_2SO_4, and HNO_3 (10 % of the background atmospheric content). Severe fires, electrified dust and aerosol releases, and depleted uranium munitions releasing uranium oxide into the

Table 15. *Waves transporting disturbances at global-scale distances*

Waves	Wave velocity (km/s)	Period (s)	Rate of absorption (km^{-1})	Propagation medium
Acoustic	$0.3 \div 0.7$	$10^{-2} \div 300$	$10^{2} \div 10^{-5}$	Atmosphere ($z \le 400$ km)
Internal gravitational	$0.3 \div 0.7$	> 300	$10^{-4} \div 10^{-3}$	Atmosphere ($z \le 400$ km)
Slow MHD	$10 \div 1$ $50 \div 5$	$10^{2} \div 10^{4}$ Same as above	$2 \cdot 10^{-3} \div 2 \cdot 10^{-4}$ $10^{-3} \div 10^{-4}$	Ionospheric E region Ionospheric F region
Seismic: longitudinal transverse	 $6.5 \div 7.5$ $4 \div 5$	 $0.1 \div 30$ Same as above	 $10^{-5} \div 10^{-3}$ Same as above	 Lithosphere Same as above
Khantadze (magneto-gradient): day night	 $\sim 0.3 \div 1$ $\sim 1 \div 5$	 $(3 \div 20) \cdot 10^{4}$ $(5 \div 54) \cdot 10^{2}$	 Not estimated Not estimated	 Ionospheric E region Same as above
Gyrotropic: day night	 $10 \div 100$ $100 \div 1000$	 $10 \div 10^{4}$ Same as above	 Not estimated Not estimated	 Ionospheric E region Same as above
MHD	~ 1000	$> 10^{-2}$	$< 10^{-5} \div 10^{-4}$	Ionosphere, magnetosphere

air, change the conductance of large enough volumes of the air, and consequently disturb atmospheric electrical parameters over the region of military operations and in the global electric circuit as whole.

A significant energetics of acoustic gravity waves produced by the wave disturbances acts to disturb coupling between the upper and lower atmosphere, as well as to give rise to the secondary processes mentioned above. Other ways also exist for the processes operating in the troposphere to affect the ionosphere and magnetosphere, and hence the entire EAIM system.

Accidents and Disasters. The geophysical effects and the ecological consequences of the explosions and fires at the ammunition dumps near Artemivsk city, Donetsk province, in October 2003 and near Melitopol city, Zaporizhia province, in May 2004 (Ukraine) are described in [22-24]. Disasters of this kind belong to those most significant under the peace. They may be treated as active experiments.

Multiple fires and explosions disturb the thermal and dynamic regime in the underlying surface-atmosphere system, when the generation, propagation, and dissipation of acoustic gravity waves activate coupling between the upper and lower atmosphere. Other ways of affecting the ionosphere and magnetosphere, i. e., the entire EAIM system, by the processes operating at the air-earth boundary cannot be excluded either.

The most important result of the study of the effects that wars and accidents at ammunition dumps have is the capability of stimulating the secondary, much more powerful, processes. The latter are caused by scattering of solar radiation by the aerosol and absorption by the soot ejected from explosions and fires into the stratosphere, which can be treated as Earth's surface partial screening. It is important that the effects of the military operations and disasters described above are characterized by the trigger gains of $10^{3} \div 10^{4}$.

4. Conclusions

1. The EAIM system has been validated to be a complex open dissipative nonlinear dynamical system. The main aspects of the system paradigm have been stated.

2. The main properties of the EAIM system include system's nonlinearity, self-development, randomness, and the appearance of triggering mechanisms for releasing energy with a triggering factor attaining in some cases $10^5 \div 10^{10}$.

3. The high-energy processes (earthquakes, volcano eruptions, thunderstorms, powerful tropospheric processes, tropical cyclones, solar terminators, solar eclipses, solar flares, geospace storms, etc.) have been shown to be the cause of the complex processes acting in the EAIM system, to give rise to rearrangement of the character of subsystem coupling, and to energy buildup and release.

It is important that the energy fluxes from above and below, as well as from anthropogenic sources can be commensurable.

4. The basic principles of major processes acting in the TAIM and OAIM systems have been developed.

5. Seismic sources and atmospheric processes affect the upper atmosphere, ionosphere, and magnetosphere via acoustic-gravity, electromagnetic, quasi-steady (electrical, magnetic) and particle precipitation channels.

6. Active experiments (explosions, rocket launches, etc.) have turned to be convenient and efficient tools for modeling subsystem coupling.

7. Wave processes play a special role in EAIM subsystem coupling.

8. Energetic electron precipitation at middle latitudes has been shown to be associated with the majority of highly variable processes operating in the EAIM system. Its fluxes can be of the order of $10^7 \div 10^9$ $m^{-2} \cdot s^{-1}$. The causative mechanisms for their precipitation have been revealed and validated.

9. The system paradigm should become the basic principle of theory, method, and methodology in the studies of the EAIM system as a complex open dissipative nonlinear dynamical one.

References

1. L. F. Chernogor, "Physics of Earth, Atmosphere and Geospace from the Standpoint of System Paradigm", *Radio Physics and Radio Astronomy*, vol. 8, no. 1, pp. 59-106, 2003.
2. L. F. Chernogor, "The Earth – Atmosphere – Geospace Environment System as an Open Dynamic Nonlinear One", *Space Science and Technology*, vol. 9, no. 5/6, pp. 96-105, 2003.
3. L. F. Chernogor, "Earth – Atmosphere – Ionosphere – Magnetosphere as Open Dynamic Nonlinear Physical System (1)", *Nonlinear World*, vol. 4, no. 12, pp. 655-697, 2006.
4. L. F. Chernogor, "Earth – Atmosphere – Ionosphere – Magnetosphere as Open Dynamic Nonlinear Physical System (2)", *Nonlinear World*, vol. 5, no. 4, pp. 225-246, 2007.
5. E. I. Grigorenko, S. V. Lazorenko, V. I. Taran, L. F. Chernogor, "Wave Disturbances in the Ionosphere Accompanying the Solar Flare and the Strongest Magnetic Storm of September 25, 1998", *Geomagnetism and Aeronomy*, vol. 43, no. 6, pp. 718-735, 2003.
6. E. I. Grigorenko, V. N. Lysenko, V. I. Taran, and L. F. Chernogor, "Specific Features of the Ionospheric Storm of March 20–23, 2003", *Geomagnetism and Aeronomy*, vol. 45, no. 6, pp. 745-757, 2005.
7. E. I. Grigorenko, V. N. Lysenko, V. I. Taran, L. F. Chernogor, S. V. Chernyaev, "Dynamic Processes in the Ionosphere during the Strongest Magnetic Storm of May 30–31, 2003", *Geomagnetism and Aeronomy*, vol. 45, no. 6, pp. 758-777, 2005.
8. L. F. Chernogor, Ye. I. Grigorenko, V. N. Lysenko, and V. I. Taran, "Dynamic processes in the ionosphere during magnetic storms from the Kharkov incoherent scatter radar observations", *Int. J. Geomagn. Aeron.*, vol. 7, 2007.
9. S. V. Panasenko, L. F. Chernogor, "Event of the November 7–10, 2004 Magnetic Storm in the Lower Ionosphere", *Geomagnetism and Aeronomy*, vol. 47, no. 5, pp. 608-620, 2007.
10. L. F. Chernogor, "The Tropical Cyclone as an Element of the Earth – Atmosphere – Ionosphere – Magnetosphere System", *Space Science and Technology*, vol. 12, no. 2/3, pp. 16-36, 2006.

11. L. A. Akimov, V. K. Bogovskii, E. I. Grigorenko, V. I. Taran, and L. F. Chernogor, "Atmospheric-Ionospheric Effects of the Solar Eclipse of May 31, 2003, in Kharkov", *Geomagnetism and Aeronomy*, vol. 45, no. 4, pp. 494-518, 2005.
12. K. P. Garmash, L. S. Kostrov, V. T. Rozumenko, O. F. Tyrnov, A. M. Tsymbal, L. F. Chernogor, "Global Ionospheric Disturbances Caused by a Rocket Launch against a Background of a Magnetic Storm", *Geomagnetism and Aeronomy*, vol. 39, no. 1, pp. 69-75, 1999.
13. V. P. Burmaka, V. I. Taran, L. F. Chernogor, "Ionospheric Wave Disturbances Accompanied by Rocket Launches against a Background of Natural Transient Processes", *Geomagnetism and Aeronomy*, vol. 44, no. 4, pp. 476-491, 2004.
14. V. P. Burmaka, V. I. Taran, L. F. Chernogor, "Wave-Like Processes in the Ionosphere under Quiet and Disturbed Conditions. 1. Kharkov Incoherent Scatter Radar Observations", *Geomagnetism and Aeronomy*, vol. 46, no. 2, pp. 183-198, 2006.
15. V. P. Burmaka, V. I. Taran, L. F. Chernogor, "Wave-Like Processes in the Ionosphere under Quiet and Disturbed Conditions. 2. Analysis of Observations and Simulation", *Geomagnetism and Aeronomy*, vol. 46, no. 2, pp. 199-208, 2006.
16. V. P. Burmaka, V. N. Lysenko, L. F. Chernogor, and Yu. V. Chernyak, "Wave-Like Processes in the Ionospheric F Region that Accompanied Rocket Launches from the Baikonur Site", *Geomagnetism and Aeronomy*, vol. 46, no. 6, pp. 742-759, 2006.
17. L. F. Chernogor, K. P. Garmash, L. S. Kostrov, V. T. Rozumenko, O. F. Tyrnov, A. M. Tsymbal, "Perturbations in the Ionosphere Following U.S. Powerful Space Vehicle Launching", *Radio Physics and Radio Astronomy*, vol. 3, no. 2, pp. 181-190, 1998.
18. L. F. Chernogor, K. P. Garmash, V. T. Rozumenko, "Flux Parameters of Energetic Particles Affecting the Middle Latitude Lower Ionosphere", *Radio Physics and Radio Astronomy*, vol. 3, no. 2, pp. 191-197, 1998.
19. L. F. Chernogor and V. T. Rozumenko, "Wave Processes, Global- and Large-Scale Disturbances in the Near-Earth Plasma", *Kinematics and Physics of Celestial Bodies. Supplement*, no. 3, pp. 514-516, 2000.
20. L. F. Chernogor, L. S. Kostrov, and V. T. Rozumenko, "Radio Probing of the Perturbations Originating in the Near-Earth Plasma from Natural and Anthropogenic Energy Sources", *Kinematics and Physics of Celestial Bodies. Supplement*, no. 3, pp. 497-500, 2000.
21. L. F. Chernogor, "Physical Processes in the Near-Earth Environment Associated with March – April 2003 Iraq War", *Space Science and Technology*, vol. 9, no. 2/3, pp. 13-33, 2003.
22. L. F. Chernogor, "Geophysical Effects and Geoecological Consequences of Multiple Chemical Explosions at Ammunition Dumps in Artemovsk", *Geophysical Journal*, vol. 26, no. 4, pp. 31-44, 2004.
23. L. F. Chernogor, "Geophysical Effects and Ecological Consequences of the Fire at the Military Base Near Melitopol City", *Geophysical Journal*, vol. 26, no. 6, pp. 61-73, 2004.
24. L. F. Chernogor, "Ecological Consequences of Multiple Chemical Explosions from a Catastrophe Caused by Man", *Geoecology. Engineering Geology. Hydrogeology. Permafrost Studies*, no. 6, pp. 522-535, 2006.

Земля – атмосфера – геокосмос как открытая нелинейная динамическая система

Л. Ф. Черногор, В. Т. Розуменко

Обоснована концепция о том, что система Земля – атмосфера – ионосфера – магнитосфера (ЗАИМ) является сложной открытой диссипативной нелинейной динамической системой, наиболее важным свойством которой являются тригерные механизмы высвобождения энергии. Сформулированы основные положения системной парадигмы. Показано, что высокоэнергичные явления в этой системе вызывают сложную совокупность процессов и перестройку взаимодействий подсистем. Активные эксперименты в системе ЗАИМ позволили установить предел линейного описания отклика подсистем на значительные энерговыделения, определить возможность возникновения крупномасштабных и глобальных возмущений от локальных и локализованных выделений энергии, а также выявить и идентифицировать типы волн, переносящих эти возмущения. Установлено, что бóльшая часть нестационарных процессов в системе ЗАИМ сопровождается среднеширотными высыпаниями энергичных частиц из магнитосферы.

Земля – атмосфера – геокосмос як відкрита нелінійна динамічна система

Л. Ф. Чорногор, В. Т. Розуменко

Обгрунтовано концепцію про те, що система Земля – атмосфера – іоносфера – магнітосфера (ЗАІМ) є складною відкритою дисипативною нелінійною динамічною системою, найважливішою властивістю якої є тригерні механізми вивільнення енергії. Сформульовано основні положення системної парадигми. Показано, що високоенергійні явища у цій системі викликають складну сукупність процесів і перебудову взаємодій підсистем. Активні експерименти в системі ЗАІМ дозволили встановити межу лінійного опису відгуку підсистем на значні енерговиділення, визначити можливість виникнення великомасштабних і глобальних збурень від локальних та локалізованих виділень енергії, а також виявити та ідентифікувати типи хвиль, що переносять ці збурення. Встановлено, що більшість нестаціонарних процесів у системі ЗАІМ супроводжується середньоширотними висипаннями енергійних частинок з магнітосфери.